
Geometric sparsification in recurrent neural networks

Wyatt Mackey
 Department of Mathematics / NIMBioS
 University of Tennessee
 Knoxville, TN 37996
 wmackey2@utk.edu

Ioannis Schizas
 DEVCOM ARL
 Army Research Lab
 Aberdeen, MD 21001
 ioannis.d.schizas.civ@army.mil

Jared Deighton
 Department of Mathematics
 University of Tennessee
 Knoxville, TN 37996
 jdeighton@vols.utk.edu

David L. Boothe, Jr.
 DEVCOM ARL
 Army Research Lab
 Aberdeen, MD 21001
 david.l.boothe7.civ@army.mil

Vasileios Maroulas
 Department of Mathematics
 University of Tennessee
 Knoxville, TN 37996
 vmaroula@utk.edu

Abstract

A common technique for ameliorating the computational costs of running large neural models is *sparsification*, or the removal of neural connections during training. Sparse models are capable of maintaining the high accuracy of state of the art models, while functioning at the cost of more parsimonious models. The structures which underlie sparse architectures are, however, poorly understood and not consistent between differently trained models and sparsification schemes. In this paper, we propose a new technique for sparsification of recurrent neural nets (RNNs), called *moduli regularization*, in combination with magnitude pruning. Moduli regularization leverages the dynamical system induced by the recurrent structure to induce a geometric relationship between neurons in the hidden state of the RNN. By making our regularizing term explicitly geometric, we provide the first, to our knowledge, *a priori* description of the desired sparse architecture of our neural net. We verify the effectiveness of our scheme for navigation and natural language processing RNNs. Navigation is a structurally geometric task, for which there are known moduli spaces, and we show that regularization can be used to reach 90% sparsity while maintaining model performance only when coefficients are chosen in accordance with a suitable moduli space. Natural language processing, however, has no known moduli space in which computations are performed. Nevertheless, we show that moduli regularization induces more stable recurrent neural nets with a variety of moduli regularizers, and achieves high fidelity models at 98% sparsity.

1 Introduction

Sparsification, or the excision of neural connections during training, is an important technique in the manufacture of computationally efficient deep learning models. Neural nets used across applications are heavily over-parameterized, and therefore both resilient to substantial sparsification and prone

to over-fitting [5, 8]. Regularization and pruning techniques have therefore found great success in improving the quality of models trained, while simultaneously decreasing the computational costs of training and running large neural architectures.

While model sparsification has been attempted using many different heuristics [9, 10, 22, 30, 36], the underlying sparse architectures are poorly understood, and vary greatly subject to small changes in both the sequence that training data is presented [6] and the initial randomization of weights [5, 8]. Frankle, et al. (2018) proposed the Lottery Ticket Hypothesis as a potential explanation of the instability of sparse models [5]. The Lottery Ticket Hypothesis suggests that sparse models arise from fortunate weight initializations on small subnetworks. Neural nets are designed to be heavily over-parameterized because this increases the probability of fortunate weight initializations on subnetworks, i.e. that some subnetwork “wins the lottery.”

This hypothesis is intuitive and appealing. However, it leaves open the problem of describing sparse neural architectures. Retraining neural nets on the so-called “winning lottery tickets” with re-randomized weights fails to recover high-quality networks in both Resnets and transformers [8]. This presents fundamental obstacles to any project of structured *ab initio* sparsity, though it does not rule out that some sparse architectures may be more stable than others. Recurrent neural nets (RNNs), however, have underlying geometric properties which may allow for greater interpretability of sparse architectures: Sussillo and Barak (2013), for instance, show that the hidden state of various low-dimensional RNNs is concentrated along *slow manifolds* of a dynamical system [38].

In this paper, we provide evidence that the geometry of RNN hidden states can be parlayed into geometric structures underlying sparse RNNs. We do this by combining magnitude pruning, in which the lowest valued weights of the neural net are thresholded during training, with *moduli regularization*. Moduli regularization, which we detail in Section 2.2, is a topologically inspired regularization term applied to the hidden-state update matrix of the RNN. It is computed by embedding hidden-state neurons into a metric space \mathcal{M} , and differentially penalizing weights according to their distance on \mathcal{M} .

This approach reflects the continuous attractor theory of RNNs [35]. The continuous attractor theory posits that the hidden layer of an RNN isolates a low dimensional parameter space (the eponymous continuous attractor, or the moduli space) of stable states, and updates at each time correspond to small movements on this space. From this perspective, moduli regularization is a method of training RNNs which favors particular embeddings of the continuous attractor into the hidden state space: specifically, embeddings which are sparse in the neural basis. By specifying neural connections based on distance on a manifold, we perform the inverse to a common strategy for manifold detection in neuroscience, in which a manifold is discovered by linking neurons that simultaneously fire [11].

We test the efficacy of our method in two recurrent architectures: a navigation RNN [37] and a natural language processing RNN [2]. In each case, we show that the choice of a well-suited moduli space and inhibitor function create superior sparse models as opposed to comparable methods. We then randomize the model’s weights and retrain the neural net on the sparse architecture to test the stability of the learned sparse architecture, showing that moduli regularization not only provides superior sparse models, but also produces sparse architectures which are more stable than alternative methods. To the best of our knowledge, this is the first paper to provide evidence of structured *a priori* sparsity in any neural architecture.

Our contributions are the following:

- We introduce moduli regularization for recurrent neural networks.
- We show that regularization premised on well-chosen moduli spaces and inhibitor functions creates superior sparse neural networks suitable for single-shot training and magnitude-based pruning. We demonstrate the effectiveness of this approach on three benchmarks.
- We provide evidence that *a priori* sparse structure can be used to train superior sparse neural nets.

1.1 Related work

Continuous attractors. Attractor dynamics in RNNs and their utility in image classification were first proposed by [35]. Many recent papers discover continuous attractors by analyzing the hidden state of trained RNNs [4, 33, 37, 38]. Similar continuous attractors, and handmade networks that

instantiate them, are common in the analysis of neural firing in the brain [1, 11, 13]. Work to encode favorable properties in RNNs, such as translation equivariance [43], are also studied in hand-crafted neural nets. However, these studies lack methods to inform the training of general RNNs with their underlying attractors.

Topology. The incorporation of parameterizing manifolds into neural network architectures has received some attention: architectures built around Grassmannians [19], symmetric positive-definite matrices [18, 21], and the Klein bottle [23] have been proposed for various tasks. These approaches are built around *a priori* knowledge of data moduli spaces, which is then built into the architecture. Other authors have attempted to combine simplicial complexes learned from the data [31] and from neural data recorded from mice [27].

Sparsity. Investigations of regularization in recent literature includes both methods focused on achievement of fixed sparsity targets [9, 10, 22, 36] and methods which sparsify differently depending on the distribution of weights [30]. However, in large models, simple magnitude pruning remains the state of the art in sparsification [8]. Training *ab initio* sparse models remains a fundamental challenge: sparse models are less stable than dense ones, meaning that random weight initializations are less likely to converge to high fidelity models [5]. Even with identical weight initializations, Frankle et al. [6] show that the stability of network training with respect to randomness in stochastic gradient descent was achieved only after a degree of training, at which point the corresponding sparsified networks agreed.

The Lottery Ticket Hypothesis of [5] is a proposed explanation for the paradox of the effectiveness of large-scale sparsification, and the ineffectiveness of training *a priori* sparse models [8]. It argues that the large over-parameterization of neural nets makes it very likely that some subnetwork is configured with a fortunate set of weights. Much past work on sparse neural nets focuses on convolutional layers of image recognition neural networks, where benchmarks are well established [8, 22, 28, 44], though attention has also been given to transformers [8, 41] and recurrent neural nets [30] for natural language processing.

2 Continuous attractors

2.1 Preliminaries

A recurrent neural net is a general term for any neural net designed to analyze sequences or streams of data, one element at a time. The Elman Recurrent Neural Network, henceforward abbreviated as RNN, is one of the most straightforward yet effective structures in common usage[4]. The RNN receives a stream of data $\{x_0, x_1, x_2, \dots\}$ represented as vectors, and maintains a hidden state H_t at each time t , a vector that functions as an internal representation of the state of the system. After an initial hidden state H_{-1} is fixed, the H_t are computed recursively as

$$H_t = s(W_{hh}H_{t-1} + W_{ih}x_t + B), \tag{1}$$

for $t \geq 0$, where W_{hh}, W_{ih} are appropriately dimensioned matrices, called the hidden update and input matrices, respectively, B is the bias vector, and s is a nonlinear function, typically tanh, or ReLU. This is represented in Figure 1(a). A decoding matrix D then takes the final hidden state, H_t , of an RNN to the desired output,

$$\text{output} = s'(D(H_t) + B_d), \tag{2}$$

where B_d is a vector, called the decoder bias, and s' is an activation function, such as the softmax (Equation (8)) for classification problems, or the identity matrix for regression problems.

An RNN can be viewed as a discrete approximation of a dynamical system on \mathbb{R}^n . It creates a vector field on \mathbb{R}^n , which is an assignment, for each point $x \in \mathbb{R}^n$, of a vector $v(x) \in \mathbb{R}^n$ such that $v(x)$ is smoothly varying in x . To flow along a vector field from a point x_0 means to take small steps in the direction $v(x_t)$ along a sequence of points $x_t = x_{t-1} + v(x_{t-1})dt$. A fixed point x of a vector field is a point with velocity $v(x) = 0$. In addition, such a point x is called stable if it flows from points in a neighborhood U converge to $x \in U$. A continuous attractor associated to a vector field \mathcal{A} is a continuous locus of stable points.

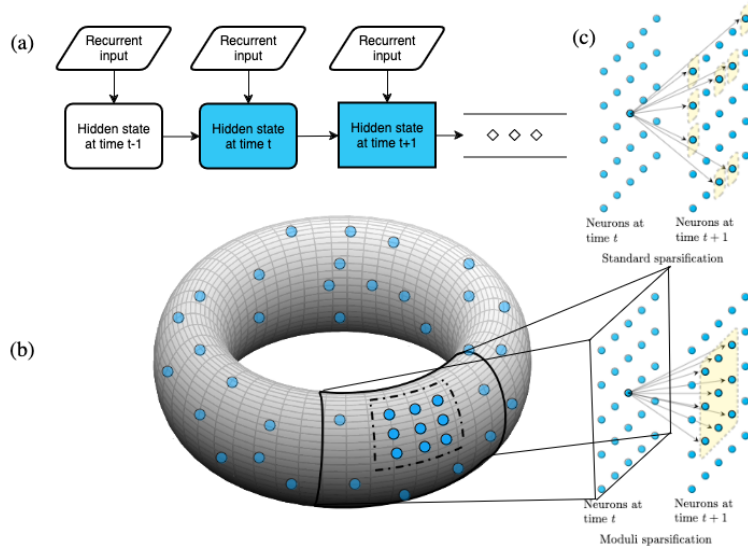


Figure 1: (a) Diagrammatic structure of the Elman RNN. (b) Hidden state neurons, represented by blue dots, are embedded into a moduli space, the torus. (c) Sparsification of the hidden update matrix of an RNN (Equation 1). Above depicts random sparsification, and below depicts sparsification in line with moduli regularization (briefly, *moduli sparsification*). Yellow boxed points are neurons with a non-zero weight connecting them to the center neuron. Moduli sparsification respects the geometry of the chosen moduli space, which is ignored by standard sparsification techniques.

2.2 Moduli regularization for RNNs

A common technique to help induce model sparsity is L_1 regularization. L_1 regularization is applied to a model $M : \mathcal{X} \rightarrow \mathcal{Y}$ with criterion $\text{criterion}(M(x), y)$ by minimizing the following loss function:

$$\text{loss}(M, x, y) = \text{criterion}(M(x), y) + \lambda \sum_{s \in S} |w_s|. \quad (3)$$

Here $\{w_s\}_{s \in S}$ is a list of all weights in the neural net and λ is the regularizing constant. More generally, we may vary the regularizing coefficient for each weight or subset of weights, as in the following sample loss function:

$$\text{loss}(M, x, y) = \text{criterion}(M(x), y) + \lambda \sum_{s \in S} c_s |w_s|. \quad (4)$$

L_1 regularization [32, 34] does not directly create sparse networks, and much work [8, 22, 28, 30, 44] has gone into creating different regularization techniques that will more directly induce sparsity. Our method, which we term *moduli regularization*, is rooted in the hypothesis that manifolds (Appendix B) usefully approximate the hidden space of RNNs.

We fix a metric space $(\mathcal{M}, d_{\mathcal{M}})$. Let $\{e_1, \dots, e_n\}$ be the standard basis vectors for the hidden state \mathbb{R}^n of an RNN, and choose an embedding $i : \{1, \dots, n\} \rightarrow \mathcal{M}$ from the set of hidden state neurons into \mathcal{M} . Let $W_{hh} = (w_{jk})_{1 \leq j, k \leq n}$ be the hidden update matrix of Equation (1). For a function $f : \mathbb{R}_{\geq 0} \rightarrow \mathbb{R}_{\geq 0}$ and $\ell \geq 1$, define an f -regularizer R_f of W_{hh} associated to the embedding i to be

$$R_f(W_{hh}) := \sum_{j, k} f(d_{\mathcal{M}}(i(j), i(k))) |w_{jk}|^{\ell}. \quad (5)$$

We depict the structure of the regularizer in Figure 1. In the figure, f is monotonically increasing for visual clarity, though this need not be true in practice (see Appendix E).

The function $f : \mathbb{R}_{\geq 0} \rightarrow \mathbb{R}_{\geq 0}$ is referred to as the *inhibitor function*. The inhibitor function is an additional parameter of the regularizer, which dictates the manner in which information is passed

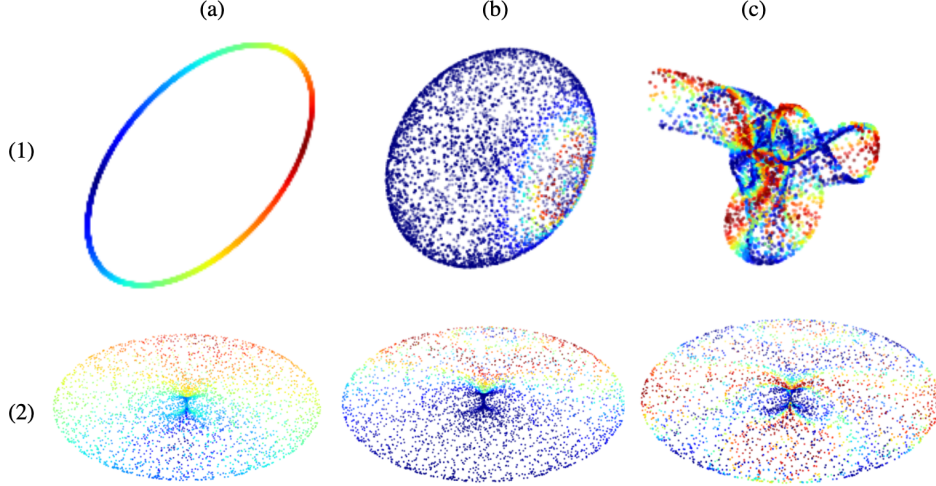


Figure 2: A neuron y is fixed. Red points depict output neurons z with low regularizing values, and therefore potentially large weights w_{yz} , while blue points are output neurons z' with high regularizing values, and therefore smaller potential weights $w_{yz'}$. Row (1) depicts the circle, sphere, and Klein bottle, while row (2) depicts the torus. Column (a) has inhibitor function $f(d) = d^2$, column (b) has inhibitor function $f(d) = 10 - 10(e^{-\frac{d^2}{5}} - e^{-d^2})$, and column (c) has inhibitor function $f(d) = 10 + 10 \cos(2d)$.

along the metric space. For example, explicit constructions of continuous attractors in neural nets for navigation [1, 13] are constructed with connectivity given by the Ricker wavelet

$$\psi(d) = \frac{2}{\sqrt{3\sigma}\sqrt{\pi}} \left(1 - \frac{d^2}{\sigma^2}\right) e^{-\frac{d^2}{2\sigma^2}}, \quad (6)$$

where d is the distance between two points on the moduli space. The attractors are unstable if simpler functions, such as $f(d) = d$, are applied as inhibitor functions, suggesting that an apt inhibitor choice is important for moduli regularizers to function. We diagram the circle, sphere, torus, and Klein bottle with various inhibitor functions in Figure 2. Further discussion and results on inhibitor functions can be found in Appendix E, and a heatmap from a trained RNN can be found in Appendix F.

A multi-layer RNN is a stack of recurrent neural networks: the first recurrent layer takes as input the input vectors x_t , as in Equation (1). Subsequent recurrent layers take as input the previous layer's hidden state H_t . We regularize each layer of multi-layer RNNs independently on the same manifold by choosing three different embeddings and using these to generate regularizers. It is also possible to change the manifold between recurrent layers, however we do not present any such experiments. Furthermore, this framework could be studied for non-recurrent architectures, although that is not the focus of the current work.

2.3 Choice of embeddings

The moduli regularizer involves the choice of an embedding $i : \{1, 2, \dots, n\} \rightarrow \mathcal{M}$ in addition to the choice of \mathcal{M} . We initialize our embeddings by drawing points independently and uniformly at random over \mathcal{M} . When \mathcal{M} has a smooth structure and the inhibitor function f is differentiable, i can be taken as a parameter of the RNN and optimized by gradient descent during the course of training.

Monotonically increasing inhibitor functions cannot be effectively used with trained embeddings: in this setting, the moduli regularizer (Equation (5)) is minimized by any embedding $\{j\}_{1 \leq j \leq n} \rightarrow * \hookrightarrow \mathcal{M}$ which maps all neurons to a single point in the moduli space. Moduli regularization then degenerates to L_ℓ regularization with regularizing coefficient $f(0)$. Other choices of f , however, such as the difference of Gaussians

$$f(x) = c - c(e^{-\frac{x^2}{\sigma_2^2}} - e^{-\frac{x^2}{\sigma_1^2}}), \quad (7)$$

where $c > 0, \sigma_2 > \sigma_1 > 0$, will not degenerate, and allow effective training of the embedding.

This has the detriment of adding $n \cdot \dim \mathcal{M}$ trained parameters to the model. However, $\dim \mathcal{M}$ is in practice always substantially smaller than n , hence the additional trained data is a small fraction of the trained data of the RNN. Additional computations are also necessary for the recalculation of the regularizing terms, however: in our experiments, we found that training the embedding resulted in substantial increases to training time. In practice it is not necessary for the embeddings to be trained: the learned update vectors will naturally adapt to randomly chosen embeddings.

3 Limitations

One flaw of our approach is that the moduli space \mathcal{M} is chosen as a hyperparameter of training, rather than adjusting to the input data. In principle it is possible for trained embeddings (Section 2.3) with $\mathcal{M} = \mathbb{R}^n$ or $\mathcal{M} = S^n$ to allow moduli spaces to be discovered simultaneously with training, but our preliminary explorations were of mixed success. Sample results from these experiments are shown in Table 3 and in Appendix H). Creating a modified training arc which allows the moduli space to be learned and detected is an interesting avenue for future research. One possible conflating factor for our experiments is our sparsification scheme—magnitude pruning. Magnitude pruning is the simplest pruning method available, and we chose it in order to simplify the discussion and avoid conflating factors in our experiments. Changes to this sparsification method might impact the level of improvement moduli regularization offers, as compared to alternative regularization schemes, though our lottery ticket hypothesis [5] experiments (Section 4) will remain of interest in this comparison. Finally, due to the computational costs, we did not extensively optimize the hyperparameters in our experiments, and tested on limited architectures.

4 Results

We test the proposed moduli regularization (Equation (5)) on two benchmark tasks: navigation and natural language processing (NLP). We study both tasks using the circle, the sphere, the Klein bottle, the 2-torus, and the 6-torus as moduli spaces, with the parameterizations described in Appendix D, and with the difference of Gaussians inhibitor function (Equation (7)). Additional data comparing other inhibitor functions is shown in Appendix E.

We chose NLP as a benchmark because it is of great general interest and is one of the most common applications of RNNs. Our original interest, however, was in the structures underlying navigation in RNNs, and navigation simulations [1, 11, 13, 33, 37] provided inspiration for our constructions. This set of benchmarks provides a useful contrast: navigation is a geometric regression task, with known moduli spaces on which the recurrent dynamics occur in both mammalian brains [1, 11, 13] and simulations [33, 37]. NLP is a classification task which lacks a clean geometric description [4]. Despite this distinction, we show that moduli regularization, particularly along the torus and the Klein bottle with difference of Gaussians inhibitors, is a highly effective technique for model sparsification for both benchmarks.

We use magnitude pruning to sparsify models during training. This means that to train models which are $p\%$ sparse over n training epochs, we threshold the lowest magnitude $(k - 1)p/(n - 1)\%$ of the model’s weights to 0 at the beginning of the k^{th} epoch. In our experiments, we chose p by running initial tests and hand selecting values at which sparse model quality was beginning to break down.

The lottery ticket hypothesis [5] suggests that sparse architectures arise from fortunate weight initializations. In other words, the training process for sparse neural architectures is unstable: the subspace of potential weight initializations which will cause training a model to converge to a high-quality net is low measure in the space of all potential weight initializations. This contrasts with dense neural nets, which are robust to random weight initializations. As a result, retraining models on a sparse architecture without using the original weight initialization deteriorates performance [5, 8]. We show that the sparse structures learned with moduli regularization are more stable than the sparse structures learned without it: models retrained on moduli-generated sparse architectures outperform models retrained on traditional sparse architectures. In several of our NLP experiments, we even achieve superior results after reinitialization and retraining *ab initio* sparse models as opposed to the original sparsified models.

Table 1: Mean navigation error in cm (standard deviation) over five experiments. Only toroidal moduli regularization accommodates 90% sparsification of the model, either during the original training or while testing the lottery ticket hypothesis.

	Torus	No reg.	L_1	Shuffled
Baseline	4.67 (0.07)	4.61 (0.04)	5.04 (0.03)	5.18 (0.07)
75% Sparse Err.	4.86 (0.30)	39.03 (41.95)	14.73 (12.23)	5.37 (0.07)
75% Lottery Err.	7.28 (0.69)	27.42 (33.28)	14.17 (2.18)	7.29 (0.81)
90% Sparse Err.	5.69 (0.43)	71.75 (32.67)	86.70 (5.95)	10.92 (0.87)
90% Lottery Err.	12.49 (2.03)	64.44 (3.81)	53.59 (9.39)	42.25 (7.65)

Table 2: Mean navigation error in cm (standard deviation) over five experiments. As a moduli regularizer, the torus, the circle, and the Klein bottle accommodate 90% sparsification, both in original training and when testing the lottery ticket hypothesis.

	Torus	Circle	Sphere	Klein	6 Torus
Baseline	4.70 (0.07)	14.47 (12.98)	35.09 (20.73)	4.73 (0.08)	8.29 (1.66)
75% Sparse	4.86 (0.30)	4.80 (0.25)	22.93 (34.16)	4.79 (0.12)	21.02 (13.25)
75% Lottery	7.28 (0.69)	6.93 (0.60)	6.45 (0.71)	6.56 (0.40)	66.75 (10.89)
90% Sparse	5.69 (0.43)	5.72 (0.71)	23.55 (35.05)	5.44 (0.13)	34.71 (16.60)
90% Lottery	12.49 (2.03)	11.02 (1.49)	28.33 (11.85)	10.96 (1.71)	93.93 (0.73)

4.1 Navigation

We study a single-layer RNN designed for autonomous landmark mapping and navigation, using the architecture of [37]. The RNN initializes its hidden state with a two-dimensional position, then takes as input a sequence of two-dimensional velocity vectors. The RNN is trained to identify which landmarks are nearest to the final position. Training data in the form of trajectories can be freely generated for the RNN, which alleviates the problem of overfitting. This allows us to study the effect of regularization on the sparsity of the underlying model, isolated from the other benefits of regularization. Hyperparameters for our experiments are listed in Appendix A.1. Trajectories occur in a 2.2 m square box, in which untrained models have a mean error of ≈ 100 cm.

Control experiments: To evaluate the utility of moduli regularizers, we compare toroidal L_1 regularization to models without regularization, with standard L_1 regularization, and with shuffled moduli regularizers. To construct shuffled regularizers, we generate moduli regularizers then randomly permute the regularizing coefficients (Equation (4)). Table 1 shows that while shuffled moduli regularizers perform well, they perform worse than moduli regularization: the inclusion of topology in the regularizing term greatly improves the sparse model fidelity. Both shuffled moduli and moduli sparsification are superior to L_1 regularization and unmodified magnitude pruning, two of the most commonly used techniques for reducing model complexity.

Moduli spaces: Table 2 compares the use of different moduli spaces in the regularizer. The torus and the Klein bottle both provide superior sparse models, comporting with their admission of \mathbb{R}^2 as a universal cover (see Appendix C). The circle also performs well, likely because $S^1 \times S^1$ is isomorphic to the torus.

Trained embeddings: In Table 3, we compare trained embeddings (as in Section 2.3) to fixed embeddings for both the torus and \mathbb{R}^3 . \mathbb{R}^3 is a space poorly suited towards navigation but contains apt moduli spaces such as the torus as a subspace. On the torus, this fails to materially improve the model. However, when \mathbb{R}^3 is used, training embeddings results in substantial improvements to the model. We additionally apply persistence homology to the trained neurons to attempt to discover what subspace of \mathbb{R}^n the neurons gravitate towards in Appendix H.

Lottery tickets: We test the lottery ticket hypothesis [5] with moduli regularizers (Tables 1 and 2) at 75% and 90% sparsity. The sparse networks that arise from moduli regularizers consistently outperform the alternatives with *ab initio* sparsity and random initializations: compare especially the columns ‘Torus’ and ‘Shuffled’ in Table 1.

Table 3: Mean navigation error in cm (standard deviation) experiments of trained embeddings in the torus and \mathbb{R}^3 over five and three experiments, respectively. Trained embeddings have little effect in an apt moduli space, such as the torus, but result in substantial improvements as opposed to randomly chosen embeddings in \mathbb{R}^3 .

	Torus trained	Torus fixed	\mathbb{R}^3 trained	\mathbb{R}^3 fixed
Baseline	4.79 (0.10)	4.67 (0.07)	5.85 (0.09)	4.77 (0.09)
75% Sparse	4.60 (0.06)	4.86 (0.30)	6.59 (0.85)	34.78 (42.10)
75% Lottery	8.20 (4.16)	7.28 (0.69)	35.44 (39.83)	60.37 (35.54)
90% Sparse	5.87 (0.55)	5.69 (0.43)	5.81 (0.45)	67.42 (33.27)
90% Lottery	15.72 (3.94)	12.49 (2.03)	20.67 (5.68)	46.56 (7.69)

Sensitivity analysis on the regularizing factor (λ in Equation (4)) can be found in Appendix G. This RNN architecture was originally introduced by [37] to study grid cells, certain specialized neurons in the entorhinal cortex which provide an internal map of space [12, 29, 42]. After the discovery of grid cells in 2005 [14], several authors [1, 13] show that toroidal neural connectivity can give rise to grid cell structures. However, to the best of our knowledge, no connectivity structures outside of the torus and \mathbb{R}^2 have been seriously investigated—the hand construction of these networks is time consuming, and small perturbations of weights can damage their effectiveness [40]. One surprising application of our moduli regularization is then the great ease with which it shows the learning advantages of the torus over arbitrary spaces, such as the sphere, for neural attractor dynamics on navigation. The success of toroidal, circular, and Klein bottle sparsification suggests that moduli regularization may provide a useful lens for exploratory work on highly structured neural connectivity. We expected these regularizers to outperform the sphere and 6-torus because \mathbb{R}^2 is a covering space (see summary in Appendix C) for the Klein bottle and the torus, making them apt compact representations for two-dimensional space. Since the torus is isomorphic to the product of two circles, a circular moduli space could also plausibly recreate toroidal connectivity.

4.2 Natural language processing

Natural language processing lacks clear *a priori* geometry to exploit [4]. Indeed, local stability of the hidden state is not a common hypothesis for NLP architectures like long-short term memory [16]. We test an RNN with three recurrent layers trained to predict subsequent words in a sequence on the Wikitext-2 dataset of high-quality Wikipedia articles [25]. Our implementation is based on the implementation of [2], which is a representative implementation of natural language RNNs. Hyperparameters for our experiments are listed in Appendix A.2.

Control experiments: To evaluate the importance of the underlying topology of moduli regularization, we compare toroidal L_1 regularization with difference of Gaussians inhibitor (Equation (7)) to models trained without regularization, with L_1 regularization (Equation (3)), and with shuffled regularization values (Table 4). Here as above, ‘Shuffled’ means that we construct a toroidal moduli regularizer, but randomly permute the coefficients of the regularizing term. At baseline 0% sparsity, toroidal moduli regularizers perform slightly worse than their shuffled version, reflecting the positive effects of random sparsification in non-geometric problems, and the importance of finding the true moduli space for NLP applications. Nevertheless, when incorporating sparsification, we find that the toroidal geometry provide some advantages compared to random sparsification. Both toroidal and shuffled moduli regularizers provide substantial improvements compared to L_1 -regularizers and non-regularized systems.

Moduli spaces: We next study an array of moduli regularizers using different moduli spaces, shown in Table 5. All experiments use the difference of Gaussians inhibitor function (Equation (7)). Unlike in navigation, our experiments show no clear preference towards specific moduli spaces, suggesting that none of our experiments reflect a true moduli space for NLP. At 90% sparsity, all moduli regularizers outperformed all control experiments, but this benefit degrades at 98% sparsity.

Lottery tickets: We test the lottery ticket hypothesis [5] for each experiment. Our results conform with the hypothesis across control experiments, indicating that the learned sparse architectures are unstable. This is also true for some—but not all—tested moduli regularizers. Several models trained with moduli regularizers *improved* after randomizing the original initialization (Circle, Sphere,

Table 4: Mean test accuracy (standard deviation) of next-word prediction RNNs at baseline, 90%, and 98% sparsity, and testing the lottery ticket hypothesis with trained sparse architectures.

	Torus	No reg.	L_1	Shuffled
Baseline	8.02% (1.73)	2.34% (0.16)	2.29% (0.03)	9.38% (0.49)
90% Sparse	10.31% (1.33)	5.30% (3.37)	2.85% (0.00)	8.44% (3.11)
90% Lottery	9.77% (0.81)	2.85% (0.00)	2.79% (0.11)	7.42% (2.49)
98% Sparse	9.59% (1.07)	2.85% (0.00)	3.78% (3.51)	9.41% (1.28)
98% Lottery	9.17% (0.51)	2.76% (0.17)	2.85% (0.00)	9.05% (0.49)

Table 5: Mean test accuracy (standard deviation) of next-word prediction RNNs at baseline, 90%, and 98% sparsity, trained with a variety of moduli regularizers, and testing the lottery ticket hypothesis. Underlined values are *ab initio* sparse models that outperform their sparsified antecedents.

	Torus	Circle	Sphere	Klein	6-Torus
Baseline	8.02% (1.73)	9.06 (1.56)	8.25 (0.95)	8.34 (1.03)	8.88 (1.26)
90% Sparse	10.31% (1.33)	9.82 (1.29)	9.41 (1.47)	9.71 (0.98)	9.83 (0.76)
90% Lottery	9.77% (0.81)	<u>10.07</u> (1.15)	<u>9.57</u> (1.12)	9.51 (0.98)	10.60 (0.64)
98% Sparse	9.59% (1.07)	10.19 (0.69)	9.36 (1.06)	8.91 (0.46)	9.26 (0.86)
98% Lottery	9.17% (0.51)	8.85 (0.34)	<u>9.48</u> (0.56)	10.09 (0.21)	8.68 (0.56)

Klein bottle, 6-Torus in Table 5), suggesting these architectures are stable with respect to weight initialization. Lacking knowledge of the true moduli space of the system results in no serious improvements compared to random sparsification (the Shuffled column of Table 4). However, the broad stability of sparse architectures produced with moduli sparsification suggests that geometric systems are more stable than non-geometric ones.

Our results show that moduli regularization remains a highly effective sparsification method in non-geometric RNNs. Moduli regularizers (Table 5) improve the accuracy of trained NLP models compared to both non-regularized and L_1 regularized models (Table 4). While they do not consistently outperform random sparsification at 98% sparsity, some moduli regularizers create sparse architectures that are more resilient to retraining with randomized weights, in some cases defying the lottery ticket hypothesis [5].

5 Discussion

We introduce a regularization scheme for recurrent neural nets influenced by the underlying stable dynamics of the recurrent system. We do this by embedding the recurrent neurons into a fixed metric space, and differentially penalizing weights according to their distance on this metric space. By embedding neurons into manifolds, we reparameterized their dynamics into sparse, geometrically organized structures. We then implemented our regularizer on navigation and natural language processing recurrent architectures, showing that it functions as a highly effective method of sparsification.

The resulting sparse networks have several features unusual in sparse neural nets. Randomly sparsified RNNs have a weakly Ramanujan sparse structure [7], meaning they are highly connected despite being sparse. This is a desirable property in network theory [17], but *not* a feature of networks sparsified with moduli regularization. Networks trained with moduli regularizers have highly correlated adjacency structures, reflecting that their connections are drawn from continuous metric spaces.

Our method is distinguished from previous sparsification methods in that it creates stable sparse models in the sense of the lottery ticket hypothesis [5, 6]. Prior work in model sparsification has found that training sparse models is heavily dependent on the weight initialization [5, 8]. Incorporating moduli regularization into sparsification alleviates these problems in some examples. In addition to creating superior sparse models, the underlying sparse architectures are *stable*: new models, with randomized initializations, can be trained on previously learned sparse architectures to high fidelity. This opens the door to future work analyzing the limitations of different sparse architectures, and the possibility of training *a priori* sparse models. Additionally, moduli regularization can be used as an exploratory technique to identify plausible candidates for manifolds underlying neural computations.

In future work, we are particularly interested in studying multi-modular regularization systems, in which different neurons are embedded in different moduli spaces, as well as adapting our work to different neural architectures. An important generalization of our work is a method which better combines manifold learning with moduli regularization to dynamically choose optimal moduli spaces for a given network.

Acknowledgments and Disclosure of Funding

This work has been partially supported by the Army Research Laboratory Cooperative Agreement No W911NF2120186.

References

- [1] Yoram Burak and Ila R Fiete. “Accurate path integration in continuous attractor network models of grid cells”. In: *PLoS computational biology* 5.2 (2009), e1000291.
- [2] Pytorch Community. *Pytorch Examples*. URL: <https://github.com/pytorch/examples/tree/main?tab=BSD-3-Clause-1-ov-file>.
- [3] Herbert Edelsbrunner, John Harer, et al. “Persistent homology-a survey”. In: *Contemporary mathematics* 453.26 (2008), pp. 257–282.
- [4] Jeffrey L Elman. “Distributed representations, simple recurrent networks, and grammatical structure”. In: *Machine learning* 7 (1991), pp. 195–225.
- [5] Jonathan Frankle and Michael Carbin. “The lottery ticket hypothesis: Finding sparse, trainable neural networks”. In: *arXiv preprint arXiv:1803.03635* (2018).
- [6] Jonathan Frankle, Gintare Karolina Dziugaite, Daniel Roy, and Michael Carbin. “Linear mode connectivity and the lottery ticket hypothesis”. In: *International Conference on Machine Learning*. PMLR, 2020, pp. 3259–3269.
- [7] Joel Friedman. “Relative expanders or weakly relatively Ramanujan graphs”. In: *Duke Mathematics Journal* (2003).
- [8] Trevor Gale, Erich Elsen, and Sara Hooker. “The state of sparsity in deep neural networks”. In: *arXiv preprint arXiv:1902.09574* (2019).
- [9] Jose Gallego-Posada, Juan Ramirez, Akram Erraqabi, Yoshua Bengio, and Simon Lacoste-Julien. “Controlled Sparsity via Constrained Optimization or: How I Learned to Stop Tuning Penalties and Love Constraints”. In: *Advances in Neural Information Processing Systems*. Ed. by S. Koyejo, S. Mohamed, A. Agarwal, D. Belgrave, K. Cho, and A. Oh. Vol. 35. Curran Associates, Inc., 2022, pp. 1253–1266. URL: https://proceedings.neurips.cc/paper_files/paper/2022/file/089b592cccfaafdca8e0178e85b609f19-Paper-Conference.pdf.
- [10] Jose Gallego-Posada, Juan Ramirez, Akram Erraqabi, Yoshua Bengio, and Simon Lacoste-Julien. “Controlled Sparsity via Constrained Optimization or: How I Learned to Stop Tuning Penalties and Love Constraints”. In: *Advances in Neural Information Processing Systems*. Ed. by S. Koyejo, S. Mohamed, A. Agarwal, D. Belgrave, K. Cho, and A. Oh. Vol. 35. Curran Associates, Inc., 2022, pp. 1253–1266. URL: https://proceedings.neurips.cc/paper_files/paper/2022/file/089b592cccfaafdca8e0178e85b609f19-Paper-Conference.pdf.
- [11] Richard J Gardner, Erik Hermansen, Marius Pachitariu, Yoram Burak, Nils A Baas, Benjamin A Dunn, May-Britt Moser, and Edvard I Moser. “Toroidal topology of population activity in grid cells”. In: *Nature* 602.7895 (2022), pp. 123–128.
- [12] Lisa M Giocomo, May-Britt Moser, and Edvard I Moser. “Computational models of grid cells”. In: *Neuron* 71.4 (2011), pp. 589–603.
- [13] Alexis Guanella, Daniel Kiper, and Paul Verschure. “A model of grid cells based on a twisted torus topology”. In: *International journal of neural systems* 17.04 (2007), pp. 231–240.
- [14] Torkel Hafting, Marianne Fyhn, Sturla Molden, May-Britt Moser, and Edvard I Moser. “Microstructure of a spatial map in the entorhinal cortex”. In: *Nature* 436.7052 (2005), pp. 801–806.
- [15] Allen Hatcher. *Algebraic topology*. Cambridge University Press, 2002.
- [16] Sepp Hochreiter and Jürgen Schmidhuber. “Long short-term memory”. In: *Neural computation* 9.8 (1997), pp. 1735–1780.
- [17] Shlomo Hoory, Nathan Linial, and Avi Wigderson. “Expander graphs and their applications”. In: *Bulletin of the American Mathematical Society* 43.4 (2006), pp. 439–561.
- [18] Zhiwu Huang, Ruiping Wang, Xianqiu Li, Wenxian Liu, Shiguang Shan, Luc Van Gool, and Xilin Chen. “Geometry-aware Similarity Learning on SPD Manifolds for Visual Recognition”. In: *CoRR* abs/1608.04914 (2016). arXiv: 1608.04914. URL: <http://arxiv.org/abs/1608.04914>.
- [19] Zhiwu Huang, Jiqing Wu, and Luc Van Gool. “Building Deep Networks on Grassmann Manifolds”. In: *CoRR* abs/1611.05742 (2016). arXiv: 1611.05742. URL: <http://arxiv.org/abs/1611.05742>.
- [20] Diederik P Kingma and Jimmy Ba. “Adam: A method for stochastic optimization”. In: *arXiv preprint arXiv:1412.6980* (2014).

- [21] Dimitrios Konstantinidis, Ilias Papastratis, Kosmas Dimitropoulos, and Petros Daras. *Multi-manifold Attention for Vision Transformers*. 2023. arXiv: 2207.08569 [cs.CV].
- [22] Christos Louizos, Max Welling, and Diederik P Kingma. “Learning sparse neural networks through L_0 regularization”. In: *arXiv preprint arXiv:1712.01312* (2017).
- [23] Ephy R. Love, Benjamin Filippenko, Vasileios Maroulas, and Gunnar Carlsson. “Topological Convolutional Layers for Deep Learning”. In: *Journal of Machine Learning Research* 24.59 (2023), pp. 1–35. URL: <http://jmlr.org/papers/v24/21-0073.html>.
- [24] Shie Mannor, Dori Peleg, and Reuven Rubinfeld. “The cross entropy method for classification”. In: *Proceedings of the 22nd international conference on Machine learning*. 2005, pp. 561–568.
- [25] Stephen Merity, Caiming Xiong, James Bradbury, and Richard Socher. “Pointer sentinel mixture models”. In: *arXiv preprint arXiv:1609.07843* (2016).
- [26] Piotr Mirowski, Matt Grimes, Mateusz Malinowski, Karl Moritz Hermann, Keith Anderson, Denis Teplyashin, Karen Simonyan, Andrew Zisserman, Raia Hadsell, et al. “Learning to navigate in cities without a map”. In: *Advances in neural information processing systems* 31 (2018).
- [27] Edward C Mitchell, Brittany Story, David Boothe, Piotr J Franaszczuk, and Vasileios Maroulas. “A topological deep learning framework for neural spike decoding”. In: *Biophysical Journal* (2024).
- [28] Dmitry Molchanov, Arsenii Ashukha, and Dmitry Vetrov. “Variational dropout sparsifies deep neural networks”. In: *International conference on machine learning*. PMLR. 2017, pp. 2498–2507.
- [29] Edvard I Moser, Emilio Kropff, and May-Britt Moser. “Place cells, grid cells, and the brain’s spatial representation system”. In: *Annu. Rev. Neurosci.* 31 (2008), pp. 69–89.
- [30] Sharan Narang, Erich Elsen, Gregory Diamos, and Shubho Sengupta. “Exploring sparsity in recurrent neural networks”. In: *arXiv preprint arXiv:1704.05119* (2017).
- [31] Christopher Oballe, David Boothe, Piotr J. Franaszczuk, and Vasileios Maroulas. “ToFU: Topology functional units for deep learning”. In: *Foundations of Data Science* 0.0 (). DOI: 10.3934/fods.2021021. URL: <https://par.nsf.gov/biblio/10303167>.
- [32] “Regression Shrinkage and Selection via the Lasso”. In: *Journal of the Royal Statistical Society (Series B)* 58 (1996), pp. 267–288.
- [33] Rylan Schaeffer, Mikail Khona, Tzuhsuan Ma, Cristóbal Eyzaguirre, Sanmi Koyejo, and Ila Rani Fiete. “Self-supervised learning of representations for space generates multi-modular grid cells”. In: *arXiv preprint arXiv:2311.02316* (2023).
- [34] Ioannis D. Schizas. “Distributed Informative-Sensor Identification via Sparsity-Aware Matrix Decomposition”. In: *IEEE Transactions on Signal Processing* 61.18 (2013), pp. 4610–4624.
- [35] H Sebastian Seung. “Learning continuous attractors in recurrent networks”. In: *Advances in neural information processing systems* 10 (1997).
- [36] Sidak Pal Singh and Dan Alistarh. “Woodfisher: Efficient second-order approximation for neural network compression”. In: *Advances in Neural Information Processing Systems* 33 (2020), pp. 18098–18109.
- [37] Ben Sorscher, Gabriel C Mel, Samuel A Ocko, Lisa M Giacomo, and Surya Ganguli. “A unified theory for the computational and mechanistic origins of grid cells”. In: *Neuron* 111.1 (2023), pp. 121–137.
- [38] David Sussillo and Omri Barak. “Opening the black box: low-dimensional dynamics in high-dimensional recurrent neural networks”. In: *Neural computation* 25.3 (2013), pp. 626–649.
- [39] Loring W Tu. “Manifolds”. In: *An Introduction to Manifolds*. Springer, 2011, pp. 47–83.
- [40] Pantelis Vafidis, David Oswald, Tiziano D’Albis, and Richard Kempter. “Learning accurate path integration in ring attractor models of the head direction system”. In: *Elife* 11 (2022), e69841.
- [41] Ashish Vaswani, Noam Shazeer, Niki Parmar, Jakob Uszkoreit, Llion Jones, Aidan N Gomez, Łukasz Kaiser, and Illia Polosukhin. “Attention is all you need”. In: *Advances in neural information processing systems* 30 (2017).
- [42] James CR Whittington, David McCaffary, Jacob JW Bakermans, and Timothy EJ Behrens. “How to build a cognitive map”. In: *Nature neuroscience* 25.10 (2022), pp. 1257–1272.

- [43] Wenhao Zhang, Ying Nian Wu, and Si Wu. “Translation-equivariant representation in recurrent networks with a continuous manifold of attractors”. In: *Advances in Neural Information Processing Systems* 35 (2022), pp. 15770–15783.
- [44] Michael Zhu and Suyog Gupta. “To prune, or not to prune: exploring the efficacy of pruning for model compression”. In: *arXiv preprint arXiv:1710.01878* (2017).

A Hardware, hyperparameters, architectures

Navigation numerical experiments were run on a NVIDIA RTX A4500 GPU with two Intel(R) Xeon(R) Gold 6246R CPU @ 3.40GHz (32 processing cores) with 640GB of memory and 28GB of swap space. The natural language processing numerical experiments were run on a NVIDIA Tesla K80 GPU with two Intel Xeon E5-2637 CPUs @ 3.50GHz (8 processing cores) with 64GB of memory and 28GB of swap space. Each navigation experiment took ≈ 2.26 hours, and each NLP experiment ≈ 2.69 hours. Our code is available at <https://github.com/mackeynations/Moduli-regularizers>

A.1 Navigation RNN

We use the same hyperparameters and architecture as [37], as listed below in Table 6, with the exception of increasing the batch size and decreasing the number of training epochs. We also remove the L_2 regularization that was applied in [37], since it substantially slows training. The code is freely available.

Table 6: Hyperparameters for navigation experiments (Section 4.1).

Hyperparameters	Values
Optimizer	Adam [20]
Batch size	200 routes
Batches tested	30 000
Sequence length	50
Learning rate	10^{-4}
Input & output dim	512
Hidden dim	4096
Bias	No
Nonlinearity	ReLU
Regularizing factor	10^{-5}
Loss	Cross entropy [24] of softmax of Gaussians
Region size	2.2 m square box

As all data was freely generated, there was no train/test split of the data: every tested path was unique.

The RNN is composed of:

1. A linear encoder for the original landmark positions
2. A linear encoder for velocity vectors
3. The hidden update matrix
4. A linear decoder from the hidden state to the relative landmark positions.

To calculate the loss, a softmax function

$$\text{softmax}([x_0, x_1, \dots, x_n]) = \left[\frac{e^{x_0}}{\sum_i e^{x_i}}, \frac{e^{x_1}}{\sum_i e^{x_i}}, \dots, \frac{e^{x_n}}{\sum_i e^{x_i}} \right] \quad (8)$$

is applied to the decoded values, which we call the predicted scores. The underlying true scores are given by $[y_0, \dots, y_n] = \text{softmax}([g_0, \dots, g_n])$, where $g_i = \frac{1}{12\sqrt{2\pi}} e^{-d_i^2/(2*12^2)}$, where d_i is the distance from the final position to landmark i . We then compare the predicted scores to the true scores using cross entropy loss:

$$\text{crossentropy}([x_i]_{i \leq n}, [y_i]_{i \leq n}) = - \sum_{i=0}^n x_i \log y_i. \quad (9)$$

The input and output functions of the RNN and the focus on landmarks is not as strange as it might appear. A very similar, though much larger, architecture was used in [26] for navigation in large

cities based purely on visual input. The rationale is that introduction of new landmarks is arbitrarily extensible, lending it greater potential generalizability of the system.

We ran a number of experiments whose results are not reported in the paper, including adding regularizers to other model parameters, and exploratory work to discover appropriate percentiles for sparsification, for which compute times were not recorded.

A.2 NLP RNN

We use the recommended hyperparameters of and architecture of [2], as listed below in Table 7. The code is available under the BSD 3-Clause License. For training and testing data, we use the Wikitext-2 dataset of high quality Wikipedia articles [25], available under Creative Commons Attribution Share Alike 3.0 license.

Table 7: Hyperparameters for NLP experiments (Section 4.2).

Hyperparameters	Values
Optimizer	SGD
Nonlinearity	tanh
Number of recurrent layers	3
Bias	Yes
Batch size	20
Embedding dim	650
Hidden dim	650
Dropout	0
Starting learning rate	20
Learning rate decay	.25
Gradient clipping threshold	.25
Backprop through time length	35

The data was split as in the Wikitext-2 dataset [25], which corresponds to roughly 82% of data reserved for training, training, 8% for validation, and 10% for test. All reported results are on the test dataset.

The RNN is composed of:

1. An encoder from the list of words to \mathbb{R}^{650}
2. Three recurrent neural layers.
3. A decoder from neural output to a one-hot encoding of the list of words.

As a loss function, we use the cross entropy (Equation (9)) of the softmax (Equation (8)) of the decoder output, as compared with the distribution which assigns probability 1 to the true next word, and 0 to all other words.

We additionally ran exploratory experiments to identify good thresholds for sparsification, for which we did not record compute time. The interested reader is recommended Tu’s (2011) book [39].

B Manifolds

A manifold is a topological space which locally is isomorphic to the Euclidean space [15]. A sphere like the earth’s surface, for example, has global curvature: it isn’t isomorphic to \mathbb{R}^2 . However, a person walking on the earth could easily mistake it as flat: a square grid is a fine way to organize something as large as a city. This motivates the following definitions:

Definition B.1. A continuous map $f : X \rightarrow Y$ is a homeomorphism if it is bijective, and its inverse $f^{-1} : Y \rightarrow X$ is continuous. We say X and Y are homeomorphic if there exists a homeomorphism $f : X \rightarrow Y$.

Definition B.2. An n -dimensional manifold is a topological space for which there exists an open cover $\{U_i\}_{i \in I}$ such that U_i is homeomorphic to \mathbb{R}^n for all $i \in I$.

Manifolds are particularly important because it is not possible to perform calculus on general topological spaces. Since manifolds are locally parameterized by copies of \mathbb{R}^n though, it is sometimes possible to perform calculus on them. This is possible whenever the homeomorphisms $U_i \cong \mathbb{R}^n$ are compatible with one another—these are known as \mathcal{C}^k manifolds, $0 \leq k \leq \infty$. \mathcal{C}^∞ manifolds are also known as smooth manifolds.

We particularly care about compact manifolds. For manifolds that are embedded in Euclidean space (for example, a sphere or torus in three dimensional space), these are spaces which contain all their limit points and are bounded. Compact spaces have the nice property that there is an upper bound on how far away pairs of points can be.

C Covering maps

Covering maps are a special class of highly controlled functions.

Definition C.1. A continuous map $f : X \rightarrow Y$ is a covering map if it is surjective and for every point $y \in Y$, there is an open set $U \subseteq Y$ containing y such that

$$f^{-1}(U) \cong \coprod_{d \in D} U,$$

where D is a discrete set. We say X is a covering space for Y .

For example, the map $p : \mathbb{R}^1 \rightarrow S^1$ from the real line to the unit circle given by

$$x \mapsto (\cos(x), \sin(x))$$

is a covering space.

Lemma C.2. If $\tilde{X} \xrightarrow{f} X$, $\tilde{Y} \xrightarrow{g} Y$ are covering maps, then $\tilde{X} \times \tilde{Y} \xrightarrow{f \times g} X \times Y$ is a covering map.

Proof. For any point $(x, y) \in X \times Y$, let $U_x \ni x$, $U_y \ni y$ be open sets in X and Y such that $f^{-1}(U_x) \cong \coprod_{d \in D} U_x$, $g^{-1}(U_y) \cong \coprod_{d' \in D'} U_y$. Then $(f \times g)^{-1}(U_x \times U_y) \cong \coprod_{(d, d') \in D \times D'} U_x \times U_y$. \square

As a result, there is a covering map $p \times p : \mathbb{R}^2 \rightarrow S^1 \times S^1$ from two dimensional Euclidean space to the torus. There is a special kind of covering map, called a universal covering map. This is a covering space $X \rightarrow Y$ where X has trivial fundamental group: that is, all loops in the space can be filled in. The interested reader is recommended Hatcher's (2005) book [15] for more details.

D Regularizer Parameterizations

To extract metric properties from the manifolds used for moduli regularizers, it is necessary to fix a parameterization. We used the following parameterizations in our experiments:

- The circle: the locus of (x, y) such that $x^2 + y^2 = 25$.
- The sphere: The locus of (x, y, z) such that $x^2 + y^2 + z^2 = 25$.
- The torus: $\mathbb{R}^2/10\mathbb{Z}^2$.
- The Klein bottle: $[0, 10] \times [0, 10]/\sim$, where \sim is the equivalence relation which identifies the points $(x, 0) \sim (x, 10)$ and $(0, y) \sim (10, 10 - y)$.
- The 6-torus: $\mathbb{R}^6/10\mathbb{Z}^6$.

To create embeddings $\{1, 2, \dots, n\} \rightarrow \mathcal{M}$ of hidden state neurons into each manifold, we sampled points independently from the uniform distribution on \mathcal{M} for each \mathcal{M} .

E Inhibitor functions

Here we provide additional data on different inhibitor functions in our experiments. For this comparison, we use the torus as a moduli space. Here c , σ , σ_1 , σ_2 , and μ are positive constants. Difference of Gaussians (DoG) and Sinusoid inhibitor functions can be natively used with trained embeddings, while Diffusion cannot without additional regularizing terms. We test using the following inhibitory functions:

- Difference of Gaussians (DoG): $f(x) = c - c(e^{-\frac{x^2}{\sigma_2}} - e^{-\frac{x^2}{\sigma_1}})$
- Diffusion: $f(x) = cx^n$
- Sinusoid: $f(x) = c + c \cos \mu x$

Results are shown in Tables 8 and 9 for navigation and natural language processing, respectively.

Table 8: Error in cm (standard deviation) of navigation RNNs (Section 4.1). The difference of Gaussians inhibitory function induces mildly superior results, as compared to alternatives

	DoG	Diffusion
75% Sparse Err.	4.86 (0.30)	4.66 (0.09)
75% Lottery Err.	7.28 (0.69)	7.05 (0.57)
90% Sparse Err.	5.69 (0.43)	14.72 (17.43)
90% Lottery Err.	12.49 (2.03)	11.32 (0.62)

Table 9: Accuracy (standard deviation) of next-word predictor RNNs (Section 4.2). The difference of Gaussians inhibitor provides substantially better results, both during sparsification and in lottery ticket experiments.

	DoG	Diffusion	Sinusoid
Baseline	8.02% (1.73)	8.72% (1.11)	2.36% (0.15)
90% Sparse	10.31% (1.33)	7.41% (3.78)	4.22% (2.87)
90% Lottery	9.77% (0.81)	6.62% (3.32)	2.85% (0.00)
98% Sparse	9.59% (1.07)	10.08% (1.01)	4.34% (3.29)
98% Lottery	9.17% (0.51)	7.62% (0.96)	2.81% (0.07)

F Heatmap for trained navigation RNN

We show a sample heatmap of the connections of one hidden neuron in our navigation RNN (Section 4.1) with moduli space the circle and inhibitor function the difference of Gaussians (Equation (7)) in Figure 3.

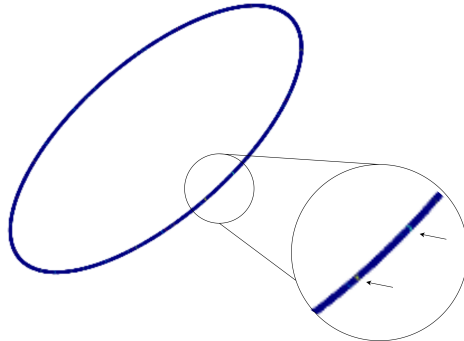


Figure 3: Heatmap of neural weights in a navigation RNN.

G Sensitivity to the weight decay factor

The influence of regularization on trained models is controlled by the weight decay constant it is multiplied by (λ in Equation (4)). We show the results of varying the regularizing coefficient λ for our navigation experiments in Table 10 and the regularizing coefficient λ for NLP in Table 11.

Table 10: We show sensitivity of the sparsification of our navigation experiments at 90% sparsity of L_1 regularization, moduli sparsification on the torus, and shuffled moduli regularizers. Here we report mean error (cm) of a single trial.

	1	10^{-1}	10^{-2}	10^{-3}
L_1 90% Sparse	92.26	92.26	86.53	90.83
L_1 Lottery	54.55	54.55	45.78	68.31
Torus 90% Sparse	5.22	5.70	5.54	5.75
Torus Lottery	79.70	13.03	30.51	51.80
Shuffled 90% Sparse	58.38	20.66	5.51	85.78
Shuffled Lottery	86.13	32.93	42.69	58.62

Table 11: We show sensitivity of the sparsification of our NLP experiment at 90% sparsity of L_1 regularization, moduli sparsification on the torus, and shuffled moduli regularizers. Here we report accuracy of the next-word prediction of a single trial.

	1	10^{-1}	10^{-2}	10^{-3}
L_1 90% Sparse	2.26%	2.85%	2.85%	1.20%
L_1 Lottery	2.26%	2.85%	2.85%	2.85%
Torus 90% Sparse	9.18%	9.94%	2.85%	2.85%
Torus Lottery	10.26%	9.82%	2.44%	2.59%
Shuffled 90% Sparse	8.32%	8.84%	8.99%	2.26%
Shuffled Lottery	9.52%	8.72%	2.85%	2.85%

H Trained embeddings to learn manifolds

To test for manifold learning with trained embeddings, we apply persistence homology [3] to navigation experiments (Section 4.1) with moduli space \mathbb{R}^3 and difference of Gaussians inhibitor function (Equation (7)) shown in Table 3. The persistence diagrams for three of the neural point cloud are shown in Figure 4. There is no clear learning of a manifold present: the neurons appear randomly distributed. For these experiments, we initialized neurons on a uniform distribution in $[0, 10]^3 \subset \mathbb{R}^3$.

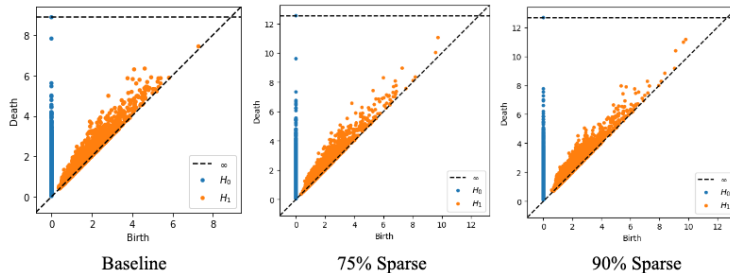


Figure 4: Persistence homology applied to neurons with trained embeddings in \mathbb{R}^3 are indistinguishable from random points.